Journal of Power Sources 233 (2013) 74–78

Contents lists available at SciVerse ScienceDirect

Journal of Power Sources

journal homepage: www.elsevier.com/locate/jpowsour

Short communication

Seed free and low temperature growth of ZnO nanowires in mesoporous TiO_2 film for dye-sensitized solar cells with enhanced photovoltaic performance

Guangwu Yang [a,b,*], Chengcheng Miao [a], Zhongheng Bu [a], Qing Wang [c], Wenyue Guo [a,b,*]

[a] College of Science, China University of Petroleum, Qingdao 266580, PR China
[b] Key Laboratory of New Energy Physics & Materials Science in Universities of Shandong, China University of Petroleum, Qingdao 266580, PR China
[c] Faculty of Engineering, National University of Singapore, 117574 Singapore, Singapore

HIGHLIGHTS

- ZnO nanowires are grown in TiO_2 film via a seed free and low temperature process.
- The hybrid film based DSCs exhibit significantly enhanced photovoltaic performance.
- The electron transport and recombination properties are studied by using EIS.
- The effects of ZnO nanowires in the hybrid film are highlighted.

GRAPHICAL ABSTRACT

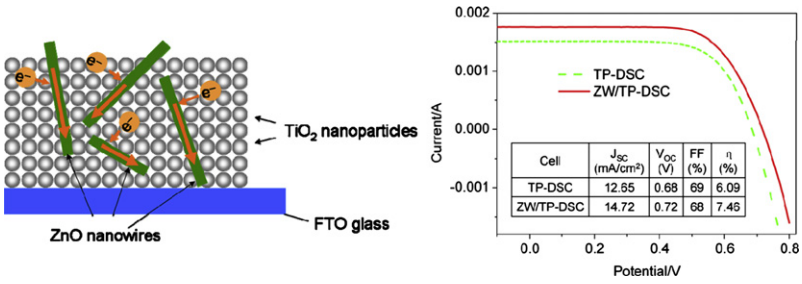

Cell	J_{SC} (mA/cm²)	V_{OC} (V)	FF (%)	η (%)
TP-DSC	12.55	0.68	69	6.09
ZW/TP-DSC	14.72	0.72	68	7.45

ARTICLE INFO

Article history:
Received 5 September 2012
Received in revised form
29 November 2012
Accepted 16 January 2013
Available online 29 January 2013

Keywords:
Zinc oxide nanowires
Hybrid films
Dye-sensitized solar cells
Post-embedding
Hydrothermal process

ABSTRACT

We report in this paper a cheap and easy method for the preparation of ZnO nanowire/TiO_2 nanoparticle hybrid films for applications in dye-sensitized solar cells (DSCs), which is achieved by post-embedding ZnO nanowires in mesoporous TiO_2 film via a seed free low-temperature hydrothermal process. The electron transport and recombination properties in the as-fabricated DSCs are studied by using electrochemical impedance spectroscopy. Results indicate that the electron transport, electron lifetime, effective diffusion length and the electron collection efficiency are increased, while the charge recombination is reduced, resulting in the remarkably enhanced power conversion efficiency of 7.46%, higher than 6.09% of standard TiO_2 nanoparticle based DSCs.

1. Introduction

Dye-sensitized solar cells (DSCs) are receiving more and more attention as one of the most promising candidates for the next-generation photovoltaic devices due to their cost-effectiveness, high theoretical energy conversion efficiency and easy fabrication processes compared with silicon-based photovoltaic devices [1]. The photoanode of DSCs usually consists of a mesoporous film based on wide-band semiconductor oxides, sensitized by a monolayer of dye molecules [2]. Upon photoexcitation, the dyes inject electrons into the conduction band of the mesoporous oxide film, the electrons then diffuse through the mesoporous oxide film network and are collected at the transparent electrode substrate [3,4]. Amongst a wide range of semiconductor oxides such as ZnO [5], SnO_2 [6], or Nb_2O_5 [7] that have been investigated previously, titanium dioxide (TiO_2) is by far the most commonly used, because

* Corresponding authors. College of Science, China University of Petroleum, Qingdao 266580, PR China. Tel.: +86 532 86981334.
E-mail addresses: yanggw@upc.edu.cn (G. Yang), wyguo@upc.edu.cn (W. Guo).

0378-7753/$ – see front matter © 2013 Elsevier B.V. All rights reserved.
http://dx.doi.org/10.1016/j.jpowsour.2013.01.087

of its chemical inertness nature that makes it an ideal supporting material for sensitizers that rely on carboxylate groups to attach the dye to the surface. A record power conversion efficiency of 12.3% for small-area laboratory test DSCs has been demonstrated recently [8]. However, the disordered pore structure of the currently used TiO_2 film has been a major factor that limits the progress of many approaches for further improvement of DSCs. The poor interconnectivity between particles results in a shorter electron diffusion length, which increases the recombination probability of the electrons with redox species [9–11].

One-dimensional (1D) nano-/microstructures may provide a solution to these challenges due to the facilitated electron transferring [9–17]. ZnO nanowires, for instances, can provide faster electron transport for the injected electrons to the back contact and shorten the electron transport pathways [12–17]. However, DSCs based on ZnO nanowires have not reached a high conversion efficiency as expected [14], which is mainly due to the insufficient surface area of the ZnO nanowires for dye adsorption compared with nanoparticles.

Constructing hybrid films based on ZnO nanowires and TiO_2 nanoparticles to take the advantages of both nanomaterials turns out to be an effective way of maintaining both high electron mobility and large surface area. In 2011, Chen et al. [16] prepared TiO_2-decorated ZnO nanorod array photoanode by a two-step approach combining hydrothermal oxidation and a sol–gel process. However, the TiO_2 sol can not penetrate the ZnO nanorod matrix, resulting in the TiO_2 nanoparticles were dominantly situated at the array top. Compared with a standard DSC that possesses a minimum power conversion efficiency of 6%, the as-assembled DSC can only exhibit a maximum power conversion efficiency of 0.94%. In 2012, Wang et al. [17] reported TiO_2 nanoparticle/ZnO nanowire array bi-film photoanode. Although the optimized DSC exhibits a high efficiency of 4.68%, the bi-filmed photoanode is essentially a mechanical alignment of two different films in tandem, which is expected of remote potential to boost the DSC performance by combining the advantages of both ZnO 1D nano-/microstructures and TiO_2 nanoparticles. The previous efforts employed the similar two-step strategy, which requires the "adding" of TiO_2 film happen posterior to the preparation of ZnO nanorod/wire film. Under the circumstances, neither the TiO_2 nanoparticles can not penetrate the ZnO nanostructure matrix to form an integrated film nor the TiO_2 film can maintain its compact and porous structure, resulting in unavoidable degradation of the TiO_2 film.

Therefore, it is most desirable to maintain both the direct conduction pathway for fast electron transfer provided by ZnO nanowires and the large surface area for sufficient dye molecules absorption offered from mesoporous TiO_2 nanoparticles. Recently, Wang et al. [18] reported seedmediated growth of ZnO nanowire network within TiO_2 nanoparticle film to prepare the hybrid film of two components for use as photoanodes, and a noticeable 26.9% improvement compared with the photoelectrode made of the benchmark TiO_2 paste is achieved. However, the fabrication of ZnO/TiO_2 hybrid film requires a laborious three-step process, involving a high-temperature pre-preparation of ZnO seed, which is not conducive to the industrialization of DSCs. In this paper, we report a cheap and easy two-step method for the preparation of ZnO nanowire/TiO_2 nanoparticle hybrid films, which is characterized by seed free, low-temperature, and less preparation time. Mesoporous TiO_2 film on FTO substrate is pre-prepared by the regularly screen printing technique, and the ZnO nanowires are subsequently embedded into the TiO_2 film via a seed free low-temperature hydrothermal method. Compared with standard TiO_2 nanoparticle based DSCs, the hybrid film based DSCs exhibit significantly enhanced photovoltaic performance.

2. Experimental

2.1. Preparation of mesoporous TiO_2 film electrode

TiO_2 film electrode is prepared by screen-printing the TiO_2 paste (Dyesol 18NRT) onto FTO glass (TEC, 15 Ω/□) several times in order to get an appropriate thickness. The printed film is then sintered in air by heating gradually to 325 °C and holding for 5 min, then 375 °C for 5 min, at 450 °C for 15 min, and finally at 500 °C for 15 min. The thickness of the film is determined by an Alpha-Step IQ surface profiler to be approximately 10 μm. No scattering layer and post $TiCl_4$ treatment are employed throughout the study.

2.2. Post-embedding of ZnO nanowires in TiO_2 film

ZnO nanowires are post-embedded in TiO_2 film via a seed free low-temperature hydrothermal process, which is conducted by immersing the TiO_2 film electrode in an aqueous solution containing 50 mM zinc nitrate ($Zn(NO_3)_2 \cdot 6H_2O$, reagent grade, 98%, Sigma–Aldrich) and 50 mM hexamethylenetetramine ($C_6H_{12}N_4$, ACS reagent, ≥99.0%, Sigma–Aldrich) and reacting at 88 °C for 12 h in an electric oven. After synthesis, the electrode is thoroughly rinsed with deionized water and allowed to dry in ambient air. The weight ratio of ZnO nanowires in hybrid film is measured by an Atomic Absorption Spectrophotometer (contrAA 700) to be approximately 7.3%.

2.3. DSC assembly

Two types of DSCs are fabricated. One is the DSC based on pure TiO_2 nanoparticle film (denoted as TP-DSC), the other is the DSC based on ZnO nanowire/TiO_2 nanoparticle hybrid film (denoted as ZW/TP-DSC). The DSC assembly process is similar to that of a standard DSC reported elsewhere [19]. The films are dyed by soaking for 12 h at room temperature in 0.15 mM solutions of N-719 (Dyesol) in a mixture of acetonitrile and tert-butanol (1:1 volume ratio). The Pt counter electrodes are prepared by depositing a thin layer of Pt nanoparticles onto the FTO substrates by thermal decomposition of hexachloroplatinic acid ($H_2PtCl_6 \cdot 6H_2O$, ACS reagent, ≥37.50% Pt basis, Sigma–Aldrich). The electrolyte used in this experiment is E008 (MPN based, 0.1 M iodine, 1 M PMII, 0.5 M NMB and 0.1 M LiTFSI).

2.4. Characterization

X-ray diffraction (XRD) patterns of the TiO_2 films on FTO substrates with and without ZnO nanowires are collected using a Rigaku D/MAX 2700 diffractometer (Japan) with Cu Kα radiation ($k = 1.5418$ Å) operating at 40.0 kV, 60.0 mA. Morphology of the ZnO nanowires are characterized by scanning electron microscopy (SEM, Philips XL 30 FEG). To estimate the dye loading on pure TiO_2 nanoparticle film and ZnO nanowire/TiO_2 nanoparticle hybrid film, the sensitized electrodes with dimensions of ca. 4 cm^2 are immersed into a 0.1 M NaOH solution (water:ethanol = 1:1), which results in the desorption of N-719. The adsorption spectra of the resulting solution are investigated by a UV–visible spectrometer (WFZ756, shanghai), and the dye loading is calculated from the absorption value for each NaOH/dye solution according to Beer's law [20].

IPCE spectra are measured with a spectral resolution of ca. 5 nm using a 300 W xenon lamp and a grating monochromator equipped with order sorting filters (Newport/Oriel). The incident photon flux is determined using a calibrated silicon photodiode (Newport/Oriel). Photocurrents are measured using an autoranging current amplifier (Newport/Oriel). Control of the monochromator and recording of photocurrent spectra are performed using a PC running the TRACQ

Basic software (Newport). The current–voltage (I–V) characterization are operated using a Keithley Source Meter and the PVIV software package (Newport). Simulated AM 1.5 illumination is provided by a Newport class A solar simulator, and the light intensity is measured using a calibrated Si solar cell. Electrochemical Impedance Spectroscopy (EIS) measurements are performed using an Autolab potentiostat/galvanostat and the Nova 1.6 software package. The cells are biased to the open-circuit photovoltage in the dark. The magnitude of the alternative signal is 10 mV, and the frequency range is from 10^5 to 10^{-2} Hz.

3. Results and discussion

3.1. Morphology and structure characterization

Fig. 1a displays the XRD patterns of the TiO_2 films before and after the hydrothermal reaction. It can be seen that after the hydrothermal reaction, the pure anatase phase TiO_2 become the composite of ZnO and TiO_2. All the diffraction peaks located at 2θ values of 20–80° for the ZnO nanowires agree well with the hexagonal phase ZnO (JCPDS No. 80-0074) without any diffraction peaks. Fig. 1b–e show the SEM images of the TiO_2 films before and after the hydrothermal reaction. It can be observed that after the hydrothermal reaction, ZnO nanowires have been successfully and uniformly embedded in the TiO_2 films, forming a hybrid film consisting of ZnO nanowires and TiO_2 nanoparticles. The hybrid film maintains the compact and porous structure of the TiO_2 film, indicating the post-embedding of ZnO nanowires does not induce any degradation of the TiO_2 film structures. The magnified image of Fig. 1d reveals that the ZnO nanowires grow in the mesopore of the TiO_2 films, with a typical diameter of 50–100 nm. To examine both the surface and the inner structure, the hybrid film is splitted (Fig. 1e). As viewed from the surface and the gap, the ZnO nanowires are highly uniform over the entire surface of and appear to extend to the full thickness of the TiO_2 film.

3.2. Photocurrent–voltage and energy conversion characteristics

Dye loading is first measured to study the effect of ZnO nanowires on the photovoltaic properties of DSCs. Fig. 2 shows the comparison of the optical absorption spectra of the dye desorbed from pure TiO_2 nanoparticle film and ZnO nanowire/TiO_2 nanoparticle hybrid film. Compared with pure TiO_2 nanoparticle film, dye loading in the hybrid film decreases from 1.6×10^{-7} to 1.2×10^{-7} mol cm^{-2}. The reduced dye loading for hybrid film can be attributed to the block of mesoporous structure by ZnO nanowires with much larger size, which subsequently leads to reduced dye loading.

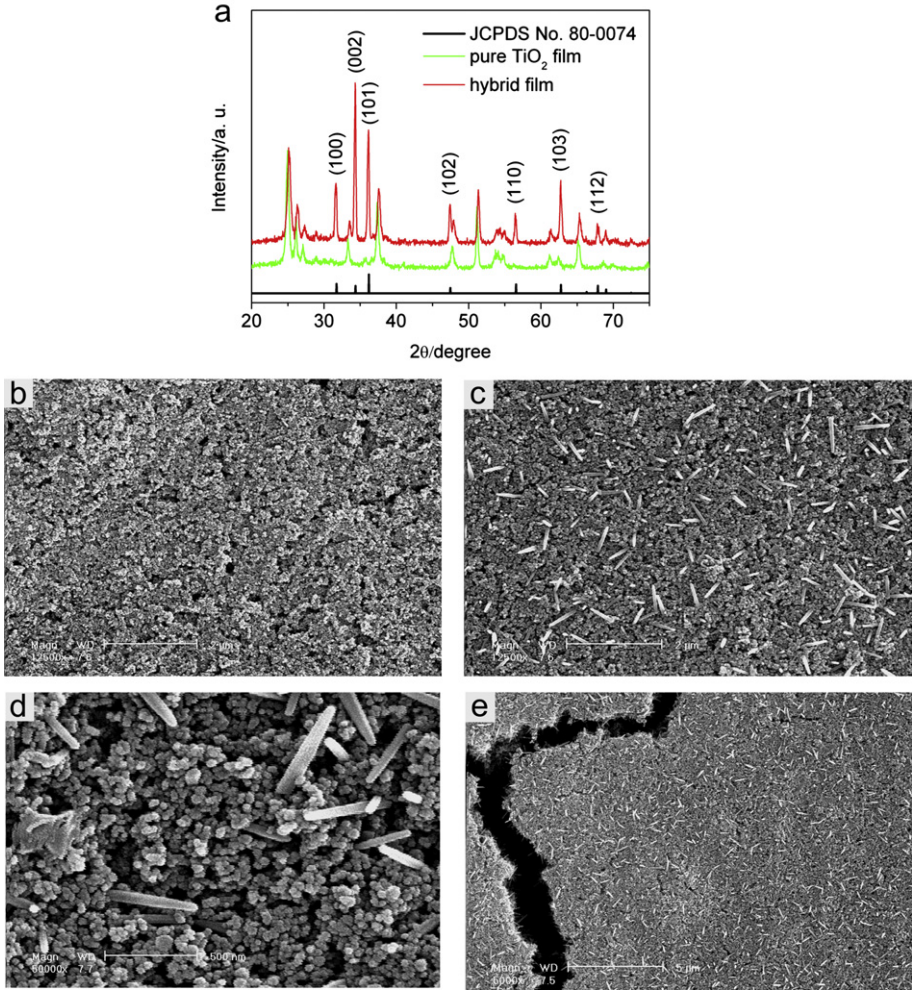

Fig. 1. XRD patterns of the reference ZnO powders, pure TiO_2 film and the ZnO nanowire/TiO_2 nanoparticle hybrid film (a), the SEM images of the pure TiO_2 film (b), and the SEM images of the ZnO nanowire/TiO_2 nanoparticle hybrid film (c–e): ((c) the overview, (d) the magnified view, and (e) the splitted hybrid film).

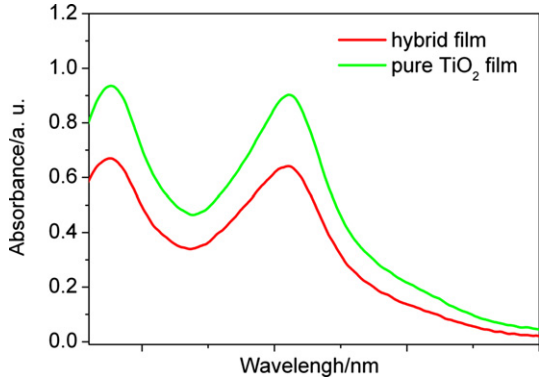

Fig. 2. Optical absorption spectra of the dye desorbed from pure TiO_2 nanoparticle film and ZnO nanowire/TiO_2 nanoparticle hybrid film the sensitized electrodes with dimensions of ca. 4 cm^2 in 0.1 M NaOH solution (1:1 ethanol and water).

Fig. 3a shows the comparison of the IPCE characteristics for the TP-DSC and the ZW/TP-DSC, both of which exhibit a broad photoresponse over the entire visible light range. The higher IPCE values of the ZW/TP-DSC rise from the reduced charge recombination benefited from ZnO nanowires that improve electron transport properties.

Fig. 3b shows the comparison of the *I–V* characteristics for the TP-DSC and the ZW/TP-DSC. The corresponding photovoltaic parameters of the DSCs are summarized in the inserted table. The J_{SC} of the ZW/TP-DSC is increased by ca. 16%, in conformity with the above IPCE results. The ZW/TP-DSC exhibits a higher V_{OC}, which can be explained by the suppression of charge recombination. Based on the increased J_{SC} and V_{OC}, the ZW/TP-DSC achieves a higher power conversion efficiency of 7.46%, which is increased by about 22% compared to the TP-DSC.

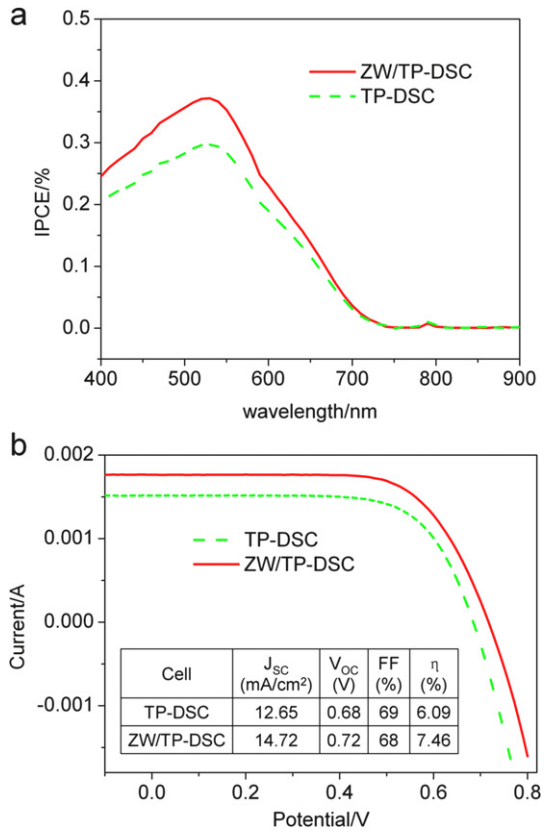

Fig. 3. IPCE spectra (a) and the *I–V* characteristics curves (b) of the TP-DSC and the ZW/TP-DSC. Inset of (b) is the summarized results of the open circuit voltage (V_{oc}), short-circuit current density (J_{sc}), fill factor (FF), and power conversion efficiency (η).

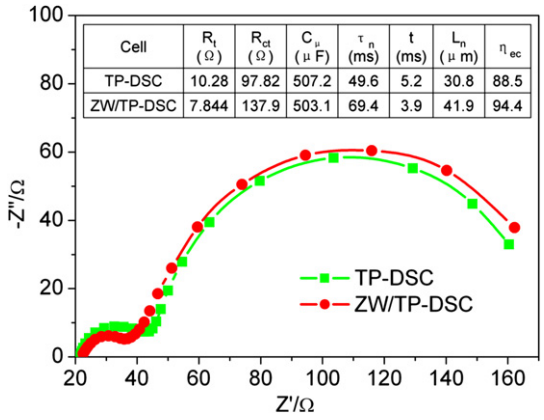

Fig. 4. Nyquist plots of the TP-DSC and the ZW/TP-DSC. Inset is the summarized results of the impedance of electron transport in TiO_2 (R_t), impedance of electron recombination with the electrolyte (R_{ct}), chemical capacitance (C_μ), electron lifetime (τ_n), electron transport time through the film (t), effective diffusion length (L_n), and the electron collecting efficiency (η_{ec}).

3.3. Electrochemical impedance measurements

Fig. 4 shows the Nyquist plots for the TP-DSC and the ZW/TP-DSC. The derived parameters are presented in the inserted table after the data being fitted by a proper equivalent circuit [21]. The decrease of R_t and the increase of R_{ct} reveal that the ZnO nanowires serve here not only as transport paths but also as trapping sites to prevent electrons recombining with the electrolyte. Therefore, an increased electron lifetime and decreased electron transport time can be observed. The smaller electron transport time in hybrid film than that in standard TiO_2 film indicates that electrons can transport fastest in the hybrid film. Moreover, the values of L_n and η_{ec} reflect the combining effects of the electron transport and the electron recombination, and the higher values of L_n and η_{ec} exhibited by ZW/TP-DSC demonstrate that the ZnO nanowire/TiO_2 nanoparticle hybrid film can enhance the photovoltaic performance of DSCs.

The above experiment observations can be explained as following: The ZnO nanowires embedded in the standard TiO_2 film can facilitate faster electron transport and at the same time retard electron recombination, which is proved the decreased electron transport time and the increased electron lifetime in hybrid film than that in the standard TiO_2 film. Thus, L_n and η_{ec} can reach higher values in hybrid film.

Fig. 5 schematically shows the electron transport process in ZnO nanowire/TiO_2 nanoparticle hybrid films. The generated electrons are collected by the nearest surface of the ZnO nanowires, which provide shorter pathways to the back contact and faster electron

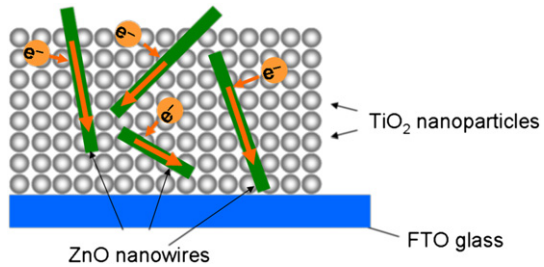

Fig. 5. Schematic diagram of the electron transport behaviors in ZnO nanowire/TiO_2 nanoparticle hybrid film.

transport for the injected electrons than the twisted interconnected TiO_2 nanoparticles.

4. Conclusions

ZnO nanowires can be successfully embedded into the mesoporous TiO_2 film via a seed free low-temperature hydrothermal process, forming a ZnO nanowire/TiO_2 nanoparticle hybrid film. The hybrid film maintains both the direct pathway for fast electron transfer provided by ZnO nanowires and the large surface area for sufficient dye molecules absorption offered from mesoporous TiO_2 nanoparticles. The ZnO nanowire/TiO_2 nanoparticle hybrid film based DSCs exhibit a remarkably enhanced power conversion efficiency of 7.46%, higher by 22% than standard TiO_2 nanoparticle based DSCs, indicating that the ZnO nanowire/TiO_2 nanoparticle hybrid film can be considered a superior material to TiO_2 nanoparticle in many respects, owing to the increased electron transport, electron lifetime, effective diffusion length and electron collection efficiency and the reduced charge recombination.

Acknowledgment

This work was financially supported by the Natural Science Foundation of Shandong Province (Grant No. ZR2011EMQ003), the Fundamental Research Funds for the Central Universities (Grant No. 11CX05004A) and the Program for Changjiang Schol-ars and Innovative Research Team in University (IRT0759) of MOE, PRC, Shandong Province Natural Science Foundation (Grant No. ZR2011EMZ002).

References

[1] B. O'Regan, M. Grätzel, Nature 353 (1991) 737–740.
[2] L.M. Peter, J. Phys. Chem. Lett. 2 (2011) 1861–1867.
[3] K. Kalyanasundaram, M. Grätzel, Coordin. Chem. Rev. 177 (1998) 347–414.
[4] M. Grätzel, Inorg. Chem. 44 (2005) 6841–6851.
[5] K. Keis, E. Magnusson, H. Lindström, S.E. Lindquist, A. Hagfeldt, Sol. Energy Mater. Sol. C. 73 (2002) 51–58.
[6] Y. Fukai, Y. Kondo, S. Mori, E. Suzuki, Electrochem. Commun. 9 (2007) 1439–1443.
[7] A. Le Viet, R. Jose, M.V. Reddy, B.V.R. Chowdari, S. Ramakrishna, J. Phys. Chem. C 114 (2010) 21795–21800.
[8] A. Yella, H.W. Lee, H.N. Tsao, C.Y. Yi, A.K. Chandiran, M.K. Nazeeruddin, E.W.G. Diau, C.Y. Yeh, S.M. Zakeeruddin, M. Gratzel, Science 334 (2011) 629–634.
[9] K. Zhu, N.R. Neale, A. Miedaner, A.J. Frank, Nano Lett. 7 (2007) 69–74.
[10] S. Gubbala, V. Chakrapani, V. Kumar, M.K. Sunkara, Adv. Funct. Mater. 18 (2008) 2411–2418.
[11] C.K. Xu, P.H. Shin, L.L. Cao, J.M. Wu, D. Gao, Chem. Mater. 22 (2010) 143–148.
[12] A.B.F. Martinson, J.W. Elam, J.T. Hupp, M.J. Pellin, Nano Lett. 7 (2007) 2183–2187.
[13] J.J. Wu, G.R. Chen, H.H. Yang, C.H. Ku, J.Y. Lai, Appl. Phys. Lett. 90 (2007) 213109–213109–3.
[14] M. Law, L.E. Greene, J.C. Johnson, R. Saykally, P.D. Yang, Nat. Mater. 4 (2005) 455–459.
[15] C.K. Xu, J.M. Wu, U.V. Desai, D. Gao, J. Am. Chem. Soc. 133 (2011) 8122–8125.
[16] T.B. Guo, Y.Q. Chen, L.Z. Liu, Y.F. Cheng, X.H. Zhang, Q. Li, M.Q. Wei, B.J. Ma, J. Power Sources 201 (2012) 408–412.
[17] M.L. Wang, Y. Wang, J.B. Li, J. Sol–Gel Sci. Technol. 61 (2012) 613–619.
[18] Y. Bai, H. Yu, Z. Li, R. Amal, G.Q. Lu, L. Wang, Adv. Mater. 24 (2012) 5850–5856.
[19] S. Ito, T.N. Murakami, P. Comte, P. Liska, C. Grätzel, M.K. Nazeeruddin, M. Grätzel, Thin Solid Films 516 (2008) 4613–4619.
[20] K. Fan, W. Zhang, T. Peng, J. Chen, F. Yang, J. Phys. Chem. C 115 (2011) 17213–17219.
[21] Q. Wang, S. Ito, M. Grätzel, F. Fabregat-Santiago, I. Mora-Sero, J. Bisquert, T. Bessho, H. Imai, J. Phys. Chem. B 110 (2006) 25210–25221.